IOP Publishing Smart Materials and Structures
Smart Mater. Struct. **26** (2017) 015004 (12pp) doi:10.1088/0964-1726/26/1/015004

Conductive magnetorheological elastomer: fatigue dependent impedance-mechanic coupling properties

Yu Wang, Shouhu Xuan, Lin Ge, Qianqian Wen and Xinglong Gong

CAS Key Laboratory of Mechanical Behavior and Design of Materials, Department of Modern Mechanics, University of Science and Technology of China, Hefei 230027, People's Republic of China

E-mail: xuansh@ustc.edu.cn and gongxl@ustc.edu.cn

Received 1 September 2016, revised 29 October 2016
Accepted for publication 1 November 2016
Published 18 November 2016

Abstract

This work investigated the relationship between the impedance properties and dynamic mechanical properties of magnetorheological elastomers (MREs) under fatigue loading. The storage modulus and the impedance properties of MREs were highly influenced by the pressure and magnetic field. Under the same experimental condition, the two characteristics exhibited similar fatigue dependent change trends. When pressure was smaller than 10 N, the capacitance of MRE could be divided into four sections with the increase of the cyclic numbers. The relative equivalent circuit model was established to fit the experimental results of the impedance spectra. Each parameter of circuit element reflected the change of fatigue loading, relative microstructure of MRE, MRE-electrode interface layer, respectively. Based on the above analysis, the real-time and nondestructive impedance method was demonstrated to be high potential on detecting the fatigue of the MRE device.

Keywords: magnetorheological elastomer, fatigue, impedance spectra, microstructure

(Some figures may appear in colour only in the online journal)

1. Introduction

Magnetorheological elastomers (MREs) are usually prepared by dispersing ferromagnetic particles into the polymer matrix. The particles were concentrated to column-like structure [1, 2], thus the MREs displayed strong anisotropy in their mechanical properties and electrical properties. In comparison to the MR fluids, MREs possessed a lower MR effect. To this end, most works on the MREs were focused on improving the MR effects and damping capability. Due to their higher stability than the MRFs', the MREs were broadly applied in various absorbers [3, 4], sandwich beams [5, 6], isolators [7, 8], etc.

The cycling mechanical property was critical for the vibration device since the MRE would be injured during the application. Carbon black was generally used to fill into the epoxy composites to predict the fatigue life and postpone the ageing problems [9–11]. In order to find out the fatigue life of MRE, the dynamic stored energy criterion was usually pre-investigated. It was reported that the dynamic fatigue properties of elastomers at constant temperature and frequency were dependent on the applied stress amplitude as well as minimum stress [12], and the change of magneto-induced modulus of MREs was related to the evolution of microstructure of filled networking [13, 14]. Zhou Y F *et al* [15, 16] investigated the influence of stress amplitudes on the fatigue, and thus developed a Wöhler curve method to determine the fatigue life in adaptive elastomeric materials. However, the mechanical testing to predict the fatigue damage or fatigue life is not real-time, and the above methods will damage the microstructure of MRE during the test.

Recent years, the conductive MREs has drawn increasing interests due to their impedance was variable to the inner structure [17–21]. The conductive ferromagnetic particles in the MRE were usually assembled to form column structure, thus the relative electrical resistance was sensitive to the externally applied magnetic field, strain or stress. Interestingly, the special piezoresistivity and the magneto-

piezoresistivity presented similar change trend with the external stimuli to the mechanical properties. Therefore, the impedance-mechanic coupling effects in the MRE became an important subject [22, 23]. Recently, various experiments and theoretical analysis were conducted to determine the relationship between the mechanics and the conductivity. Typically, Borin, D Y *et al* [24] showed that the composite based on a silicon polymeric matrix with embedded magnetic particles coated with a polymeric dielectric shell was highly sensitive to both magnetic and electric fields. In order to fully understand the mechanism of field-dependent conductivity of MR material, a simple theoretical model was also proposed to predict the conductivity under the magnetic field [25]. Based on an ideal assumption of perfect chain structure, the current flowing through the chain structure consists of both tunnel current and conductivity current, both of which depends on external loadings [26].

The real-time impedance measurement for MRE could be very easily achieved due to the simplicity of testing process. Since the coupling effects between the impedance and mechanic characteristic, the physical state of the MRE during the application would be obtained by testing the conductivity [27–29]. The influence of the external stimuli and cycling loading on the impedance played a key role on the sensitive performance of MRE. Unfortunately, the fatigue dependent impedance of the MREs has not been intensively investigated. Moreover, the relationship of the conductivity, mechanical properties, and microstructure during the cycling loading was still a critical problem. Previously, the SEM [30–33], synchrotron radiation x-ray computed tomography [34, 35], digital image methods were developed to investigate the inner microstructures of MRE and studied their geometrical properties [36]. However, the above methods could not give out the change of interface between the particles and the matrix. The impedance was sensitive to the microstructure change by displaying resistance or capacitance. Therefore, the impedance spectra is estimated to be an effective method to detect the structure change during the cycling loading.

In this paper, we investigated the impedance change of the MRE samples under different fatigue loading. Same to the mechanical characteristics, the electric properties of the MRE varied with the loading cycles due to the change of the microstructure [37–39]. The dependence of cycling loading on both the mechanical and electrical properties was investigated and the detailed mechanism was discussed. Since the simplicity of the testing process, the non-destructive impedance spectrum method presented high potential in real-time detecting the damage of the MRE microstructure and predicting the fatigue life in practical application.

2. Experimental section

2.1. Preparation of MREs

In this experiment, natural rubber (NR, type SCR WF, from Hainan Rubber Group in China) based MREs with carbonyl iron (CI, type CN, from BASF in Germany) particles weight fractions of 85% were prepared. The average diameter of CI particles was 6 μm. Rosin glycerin ester was selected to decreased the viscosity of rubber matrix, provided by West Tech Chemical Co. Ltd in China [40]. Plasticizers were composed of half dimethyl phthalate and half white vaseline, and the vulcanizator was composed of sulphur. All the reagents were analytical pure and were used without additional purification.

In order to keep simplicity and accuracy in building the model and analyzing, and ensure a clear electrical feedback after thousands of cyclic loading, no conductive materials except CI particles was added in the MREs. All the components were mixed homogeneously by using a two-roll mill (Taihu Rubber Machinery Inc. China, Model XK-160), and the mixture was compressed into molds. Then, the molds were set under an external magnetic field of 1.5 T to pre-structure for 15 min and cure for 20 min The environmental temperature of the pre-structure and cure process were 80 °C and 153 °C, respectively. In this research, the dimensions of MRE samples for dynamic mechanical tests were 10 mm × 10 mm × 5 mm, and for electric tests the diameter was 10 mm and height was 20 mm. The direction of the magnetic field was perpendicular to the bottom surface of the sheet or cylindrical MREs. Therefore, the CI particles were assembled to form chain-like structures in the matrix.

2.2. Test system and methods

The MREs were set into a cyclic loading tester (JC-1008, JiangduJingcheng Test Instruments Co.) and loaded with sinusoidal compression like most of the practical application (figure 1(a)). The load direction was parallel to the direction of particle chains. The frequency was 300 rad min^{-1} and the strain was set as the 20% of the height of samples. The MREs' mechanical and electric properties were tested after loading 0, 2×10^3, 4×10^3, 6×10^3, 8×10^3, 10×10^3, 12×10^3 and 14×10^3 cycles.

The mechanical performance was measured with a modified dynamic mechanical analyzer (DMA, Triton Technology Ltd, UK, model Tritec 2000B). A self-made electromagnet was attached to the DMA, which could generate a variable magnetic field from 0 to 800 mT. The testing frequency swept from 4 to 19 Hz, and the shear strain amplitude was set at 0.1%. The load direction was vertical to the particle chains.

The morphology of MRE samples were characterized by scanning electron microscopy (SEM, Philips of Holland, model XL30 ESEM-TMP), operating at 20.0 kV. Each sample was cut into flakes and coated with a thin layer of gold for observation.

We set up an electrical test system (figure 1(b)) combined with the Modulab material test system (MTS, Solartron analytical, AMETEK advanced measurement technology, Inc., United Kingdom) and the Electromechanical universal Testing Machine (Model 43, MTS System Corporation, China). The cylindrical MREs were adhered to the polished copper plates by the conductive adhesives (Type DAD-40, Shanghai Research Institute of synthetic resins, China), and stayed for

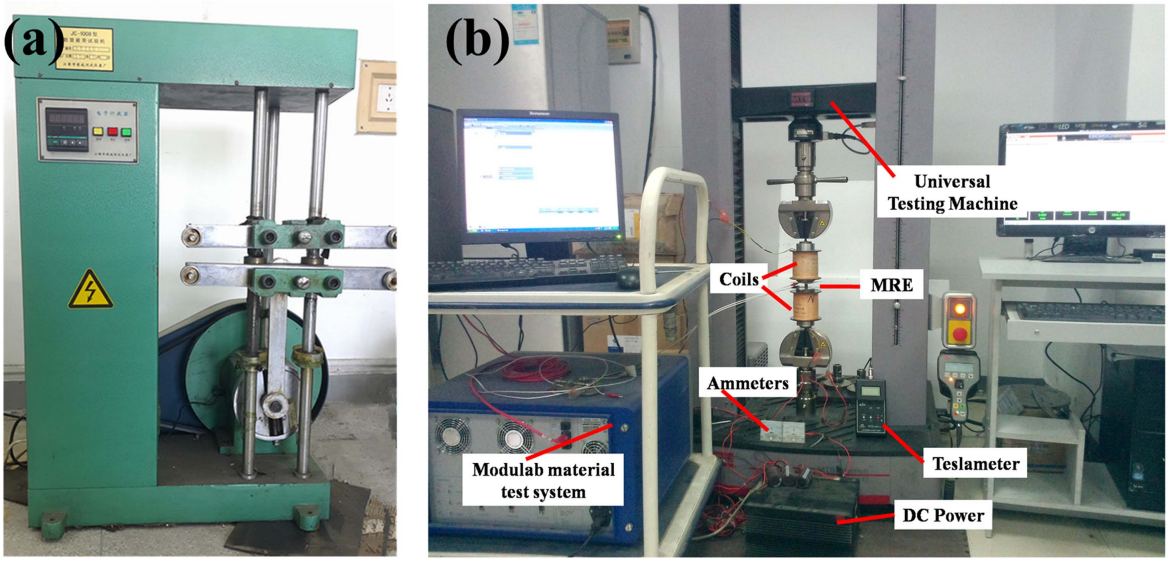

Figure 1. The cyclic loading tester (a) and the electrical test system (b).

24 h under a certain pressure at room temperature to finish connection. It should be noted that the oxide layers on the copper plates surface had a great influence on the impedance spectra measurement.

The stress loaded on MRE was controlled by the computer and the relationship between the force and displacement was measured. During the stress loading, the system generated excite voltage and measured the response voltage or current. The alternating current (AC) voltage amplitude was set at 2000 mV, so as to avoid some date jitter caused by the power source. A teslameter (type HT20, Shanghai Hengtong magnetic technology Co., Ltd, China) was used to measure the magnetic field strength. The MREs were loaded from 0 to 30 N, and once reached a certain value, it was kept for 2 min until it became stable and then tested. The frequency of AC was set to sweep from 1000 kHz to 1 Hz.

3. Result and discussion

To comprehensively understand the MRE microstructure change after cyclic loadings, SEM images were used to investigate the microstructure. As illustrated in figures 2(a) and (b), the white spherical particles were CI particles, and the fibers were NR rubber. All the MREs exhibited chain-like structures which were parallel to the external magnetic field direction, and they were bonded well with the NR rubber matrix. During the prestructure process, the CI particles moved from isotropic to anisotropic, thus the fibers were almost paralleled to the magnetic field (figure 2(a)). Because of the high content of iron particles, the particle chains were close to each other. As shown in figure 2(b), after cyclic loadings, the chain-like structures were disturbed and the aligned structures became less regular than before. Especially, most of the rubber fibers had the irregular shape and the chain-like structure was shorter and more uneven. Obviously, the inner structure of the MRE was partly broken by the cycling loading. Although the micro cracks especially between the particles and the matrix cannot be observed through SEM images, it could be deduced that the mechanical and electrical properties were changed regularly with the fatigue of MREs.

The mechanic properties of the MREs after cyclic loadings were tested by the DMA. Keeping the shear frequency at 4 Hz, when the number of cyclic loading was 2000, the storage modulus increased from 9.3 to 21.6 MPa with increasing of the magnetic field (figure 2(c)). If the cyclic loading number reached 14 000, the storage modulus rose from 6.8 to 14.7 MPa. The magneto-induced storage modulus is defined as $\Delta G = G - G_0$. Here G_0 is the initial storage modulus, and G is the storage modulus under different magnetic field. When the cyclic loading number was 14 000 and the shear sweeping frequency was at 4 Hz, 7 Hz, 10 Hz, 13 Hz, 16 Hz and 19 Hz, the magneto-induced storage modulus varied 4.9 MPa, 4.8 MPa, 4.5 MPa, 4.7 MPa, 4.8 MPa and 4.4 MPa respectively, and the MR effect decreased 19.4%, 18.8%, 15.2%, 18.5%, 19.9% and 15.5% respectively. Typically, with increasing of the cyclic loading numbers, the sweeping frequency had more impact on the shear storage modulus. After loading for 2000 times, G_0 rose 10.8% and the G_{max} rose 4.7% when the sweeping frequency increased from 4 to 19 Hz. And when loading 14 000 times, G_0 rose 14.7% and the G_{max} rose 8.5%. Here, after the fatigue loading, the deformation/ruptures of the rubber fibers (figure 2(b)) and the destruction of the chain-like structure led to the decrease of the storage modulus and the increase frequency effect on the modulus. In addition, slippage was more easily to happen between particles and matrix, which also resulted in the above phenomenon.

Figure 3 showed the influence of cyclic loading times on the initial modulus of the MREs under different shear frequency scanning. When frequency was at 4 Hz, the storage modulus fell with the cycling loading from 9.4 to 6.3 MPa

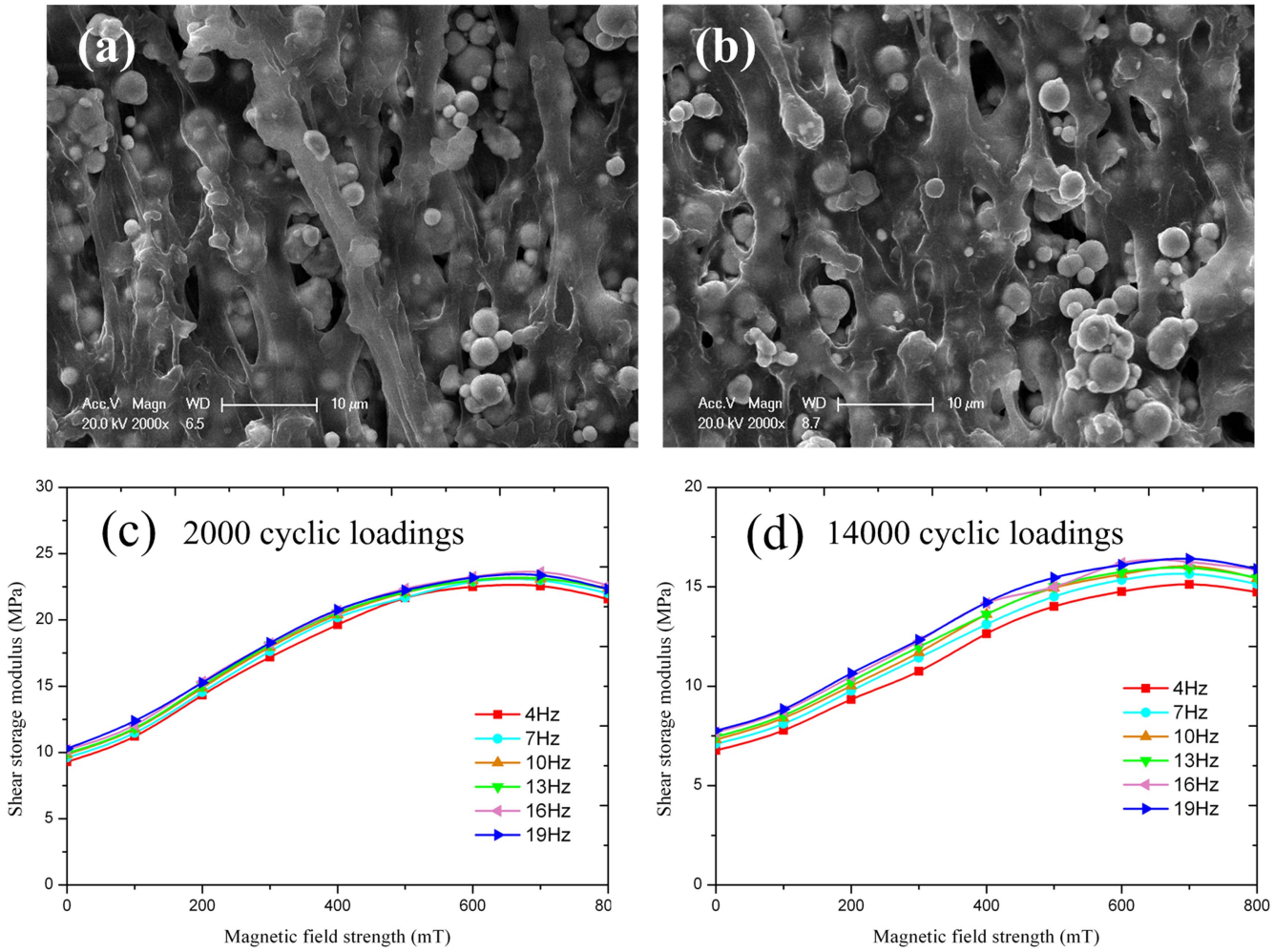

Figure 2. The SEM images of MRE samples and its relative shear modulus: (a), (c) after 2000 times cyclic loading; (b), (d) after 14 000 times cyclic loading.

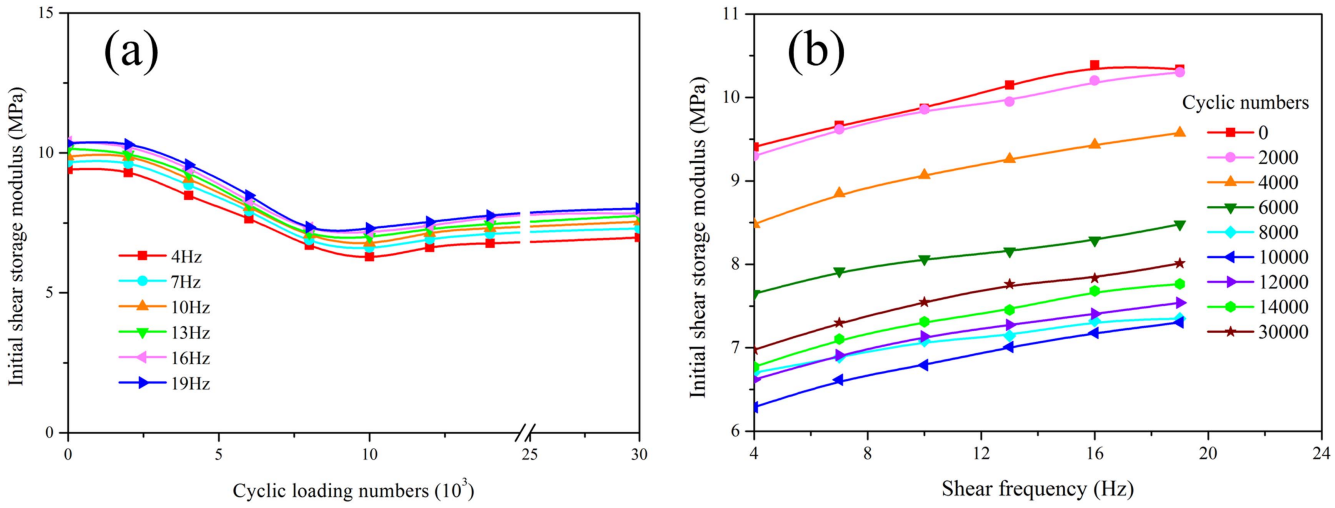

Figure 3. The initial storage modulus of MRE: (a) under different shear frequencies; (b) after different cyclic loading numbers.

within 1×10^4 times loading. However, once after 1×10^4 times, the modulus slowly rose, and gradually increased to 7.0 MPa until after 3×10^4 times loading. In this case, the shear frequencies barely affected change. Before 1×10^4 times loading, the change of the modulus was due to the destruction of the microstructure and the slippage between the matrix and the particles. With increasing of the cycle numbers, the plastic deformation became severer, led to the

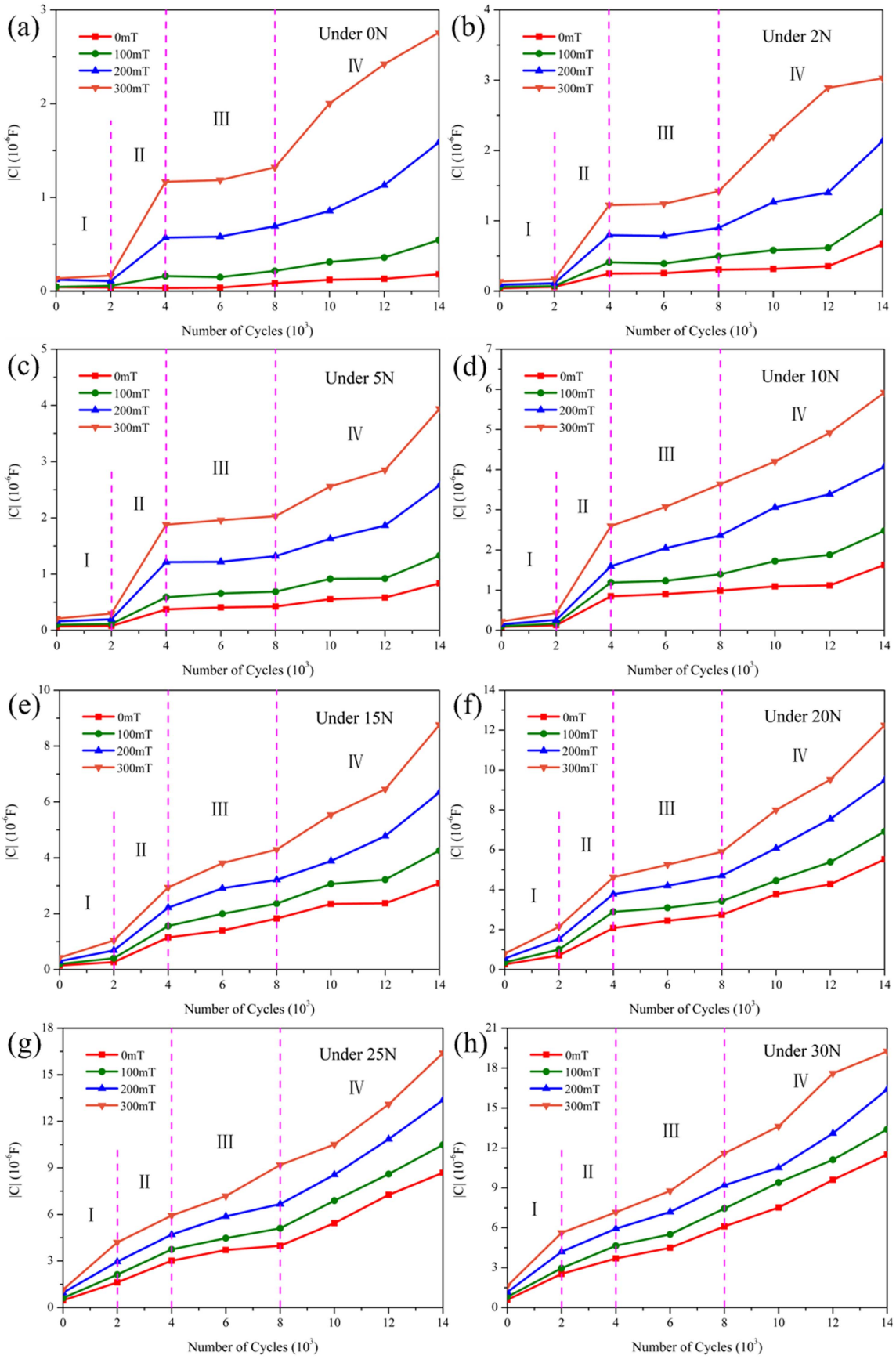

Figure 4. The relationship between capacitance of MRE and cyclic loading numbers under different pressure loading and magnetic field strength: 0 N(a); 2 N(b); 5 N(c); 10 N(d); 15 N(e); 20 N(f); 25 N(g).

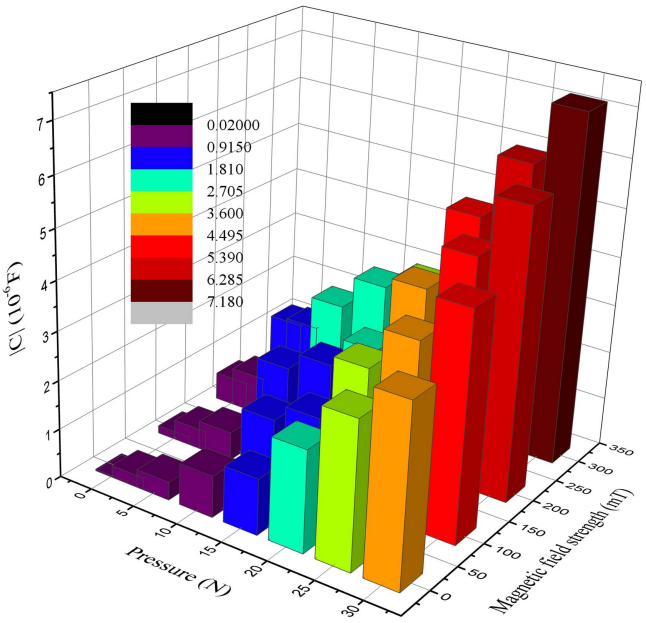

Figure 5. The capacitance of MRE after 4000 times cyclic loading.

decrement of the MRE sample height and the distance of adjacent particles. This reason had more dominant effect with the cycle loading increased, so the modulus rose gradually after 1×10^4 times loading.

Because it was harmful and laggard for MRE to forecast the life span of MREs or judge the change even damage of the microstructure through measuring the shear storage modulus, so we tested electrical performance to compensate these defects. We conglutinated two copper polar plates on both bottom surfaces of the cylindrical MRE with the conductive adhesives and established a capacitor. Then, we measured the capacitance change of MREs under different external magnetic field and pressure loading, which had endured different degree of fatigue loadings. At high frequencies, the electrons were sufficiently excited so that they can hop from one conducting cluster to another because of the smaller interparticle gap [41].

As figure 4 shown, when pressure was smaller than 10 N, the curves of capacitance could be divided into four sections with the increase of the cyclic numbers. When MRE was compressed before 2×10^3 times (stage I), capacitance was stable at a small value. Then, the curves soon increased when MRE was compressed between 2×10^3 and 4×10^3 times (stage II). The stage III ranged from 4×10^3 to 8×10^3 times, in which the change of capacitance came back to be steady and rose slowly. Figure 5 showed the capacitance of MRE after 4000 times cyclic loading, and the magneto-mechanical coupling behavior was carried out. Finally, the region when loaded over 8×10^3 times was stage IV and the curves began to rise significantly. The greater the magnetic field strength was, the more obvious these performances of MRE would be. However, with the numbers of cycles further increased, the sections of the capacitance curves began to be uniform and showed a trend of rising gradually.

The capacitance of the MRE experienced a similar change process to the mechanical performance during the cycle loading. The platform segment of the curves correlated to the yield stage of MRE. In the first stage, MRE was stable and no structure destroy was happened. Under applying different magnetic field strength, little difference was found since the good combing of particles and rubber matrix fibers. In the second stage, the MRE began to appear a low fatigue, and the deformation happened. In the third stage, materials entered the yield stage. While the space between adjacent particles continuously reduced, the structure was damaged. In the last stage, intense plastic deformation occurred. The decrease of interparticle spacing and the increase of the surface contact became the dominant factor of the capacitance change. The cyclic loading increased the distance that the particles could move, so the capacitance rose gradually. With increasing of the pressure, the platform segment of curves (stage III) was fade away gradually and the yield stage was skipped. When pressure was larger than 10 N, the decrease of interparticle spacing caused by plastic deformation led to the rising of the capacitance. So the division of the four stages became less and less obvious. Based on the above analysis, it was found that the platform segment disappeared earlier with increasing of the magnetic field. This phenomenon was responded for the larger magnetic contraction in the higher magnetic field strength.

Figures 6(a)–(c) represented the impedance spectra of MREs after different fatigue loading. If the pressure was 0 N, resistance rose from 3.7 to 4.9 MΩ when the number of fatigue loading increased to 4000. After 4000 times, the resistance began to decline, and gradually became stable. With the increase of pressure (5 N), the resistance declined directly and quickly once the cyclic mechanical loading started, and leveled off earlier. When the testing pressure continued to increase and reached 20 N, the resistance began fell much more sharply once the degree of fatigue increased, and the resistance when tended to be stable significantly reduced. This was mainly due to the internal stress existed during the pre-structure and vulcanization process. The distortion of structure caused by the internal stress was released and recovered after a certain degree of fatigue loading. Therefore, the resistance had a rising process. Under applying the external pressure, the stress was much greater than the internal stress, so the deformation caused by the external pressure decreased directly. In addition, the greater the degree of fatigue, the more micro structure would relax under the pressure, and the faster to reach stable. In the absence of pressure load, with increasing of the fatigue degree, the impedance arcs tended to be more and more semicircular, and the small section arcs at high frequencies gradually disappeared. During the sample preparation, the distribution of iron particles along the direction of chain structures was unavoidably uneven in the most cases. While the number of fatigue load increased, the plastic deformation and readjustment of the internal structure led to the particle distribution along the chain to be uniform gradually. Therefore, the small section arcs attributed from the non-uniform dispersion disappeared under long fatigue loading.

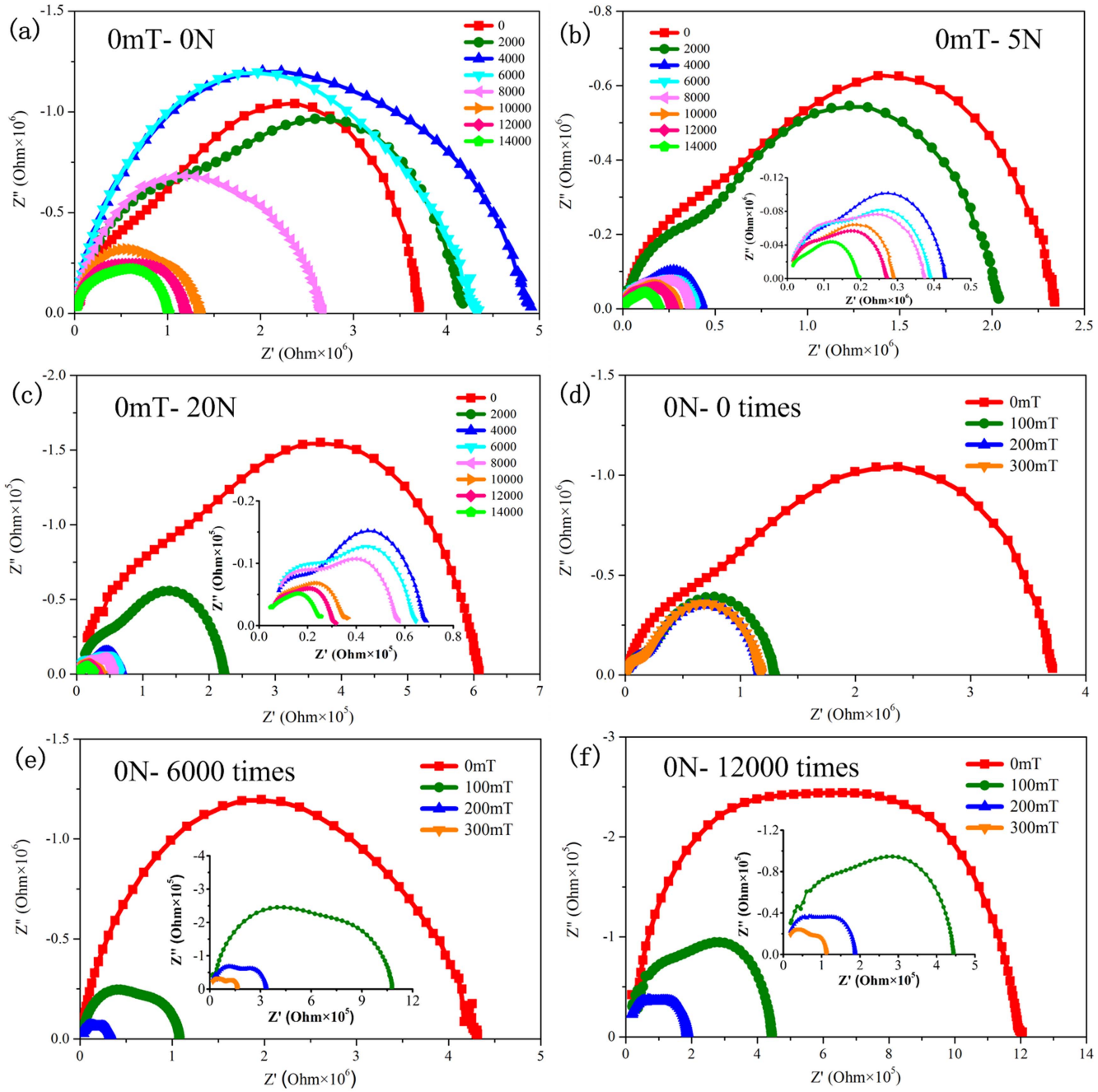

Figure 6. The impedance spectra of MREs after different fatigue loading when tested in the absence of magnetic field or pressure loading: (a) 0 mT-0 N; (b) 0 mT-5 N; (c) 0 mT-20 N; (d) 0 N-0 times; (e) 0 N-6000 times; (f) 0 N-12000 times.

Figures 6(d)–(f) represented the impedance spectra of MREs under different magnetic field strength. Without the fatigue loading, the impedance quickly changed under applying the external magnetic field. When the magnetic field was increased from 100 to 300 mT, the change of the impedance spectra was inconspicuous and gradually reached a platform. However, when the fatigue loading was 6000 times, the resistance decreased significantly with the increase of the magnetic field intensity. When the fatigue loading numbers reached 12 000 times, the resistance of MRE without applying any magnetic field decreased to 1.2×10^6 Ω. However, due to the relative slippage of the microstructure, the increasing magnetic field still had a big influence on the resistance.

If only pressure was present, the shape of the impedance spectrum gradually changed toward a semicircle with the increase of the pressure loading. However, when only applied magnetic field, the shape of the impedance spectrum gradually consisted of two segment of arcs. Because of the magnetic contraction, the particles gradually move towards the sample center area under the magnetic field [38]. The area around the bottom surface was more obvious instead where particles were few (figure 7). At this point, when the impedance spectrum consisted of two segments of arcs, it could be

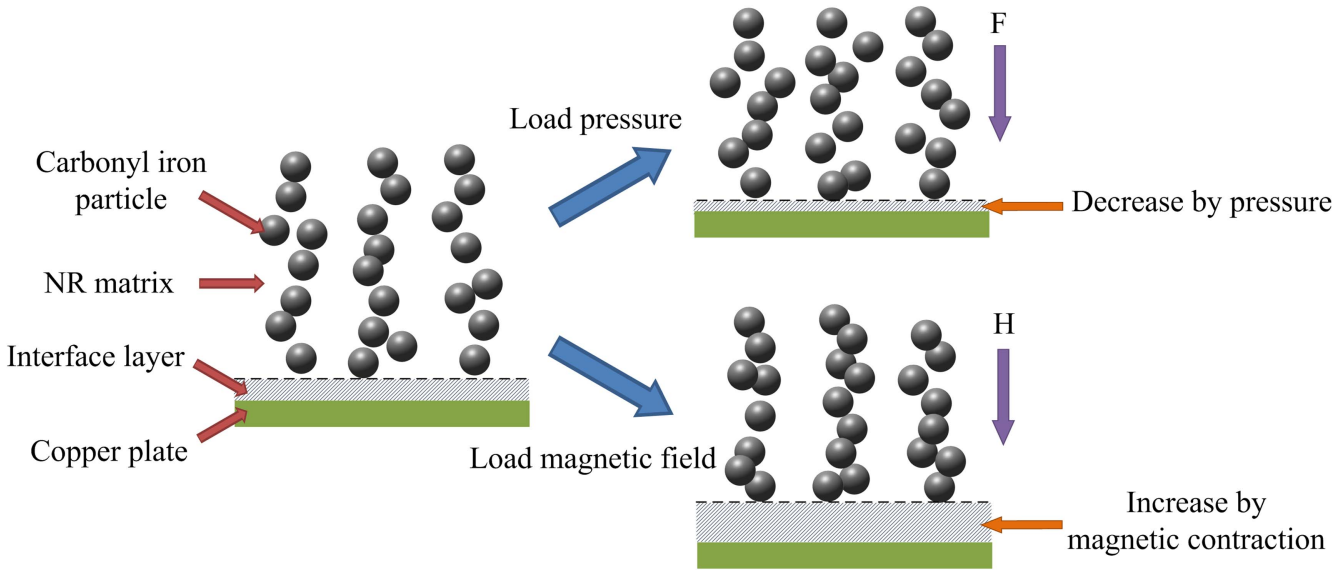

Figure 7. The schematic of MRE and MRE-electrode's change under pressure or magnetic field.

regarded that the specimen consist of two different components: the MRE center area and the MRE-electrode interface layer. This trend was not obvious if the fatigue loading number was smaller than 6000 (figure 6(e)). At this stage, particles and matrix still contacted well, so that the moving of the particles caused by magnetic contraction was limited. When the fatigue loading reached a certain degree, with the increase of magnetic field strength, two peaks began to appear in the impedance spectra of MRE.

The equivalent circuit model was established to fit and analyze the electric response of MRE under external pressure loading and magnetic fields. As shown in figure 8(a), the equivalent circuit model was composed of the resistance R_1, R_2, and the constant phase angle element CPE_1, CPE_2. Two groups of circuit elements in parallel represented the electric properties of MRE and the MRE-electrode interface layer, respectively. Through fitting the Nyquist plots, we obtained the values of each circuit element parameter. Thus, the MRE properties and the change of the microstructure under different cyclic loading could be obtained and analyzed.

The figures 8(a)–(c) showed the relationship between the resistance elements R_1 and cyclic loading numbers under 5 N(a), 15 N(b) and 25 N(c). The electron conduction through the particles strongly dependent on the interparticle distance and roughness on the particles surface [42]. It could be considered that the R_2 represented the resistance of MRE sample, while the R_1 represented the resistance of the MRE-electrode interface layer [39]. When the pressure was 5 N, R_1 firstly decreasing slowly and then the tendency accelerated to decline. With increasing of the magnetic field, even the tendency increased first and then decreased appeared. When the magnetic field was at 300 mT, R_1 rose from 1.9×10^5 to $2.0 \times 10^5\,\Omega$, and then declined to $6.7 \times 10^4\,\Omega$ directly. When the pressure increased, this phenomenon disappeared gradually. In addition, the descent rate would be faster when the cyclic loading number was less than 4000, and tended to be stable sooner. This was mainly because the compression stress on the interface was much more obvious, and a certain degree of fatigue made the microstructure change more easily.

Differently, R_2 decreased more slowly than the $R1$ with the increase of fatigue loading numbers (figures 8(d)–(f)). Therefore, the place where fully compression happened first when loading force was the MRE-electrode interface layer. The particles' concentration in the surface layer of specimen was smaller than the inner, so the modulus was lower. With increasing of the loading pressure, the influence of magnetic field strength on the resistance became smaller. It was attributed to the adjacent iron particles got close to each other gradually when the pressure increase. The move range of the CI particles was small and the magnetic contraction was also greatly limited, so the magnetic field exhibited less effect on the microstructure.

The resistance was difficult to reflect the damage degree of MRE, especially under pressure, thus the CPE-T of the constant angle element was investigated. CPE_1-T represented the capacitance of the MRE-electrode interface layer and each tiny damages caused by relative displacement would play an important role in the capacitance. As shown in figures 9(a)–(c), keeping the pressure at 5 N, CPE_1-T was stable before 10 000 times fatigue loading. Once after 12 000 times, CPE_1-T increased. The increasing amplitude became more and more obvious with the magnetic field. When the magnetic field was larger than 300 mT, the huge change indicated that the interface was damaged. The microcracks reduced the dielectric constant of the medium directly and magnetic contraction enlarged the microcracks, which resulted in a sharply increasing of the capacitance. Particles' concentration at this place was small, so the microstructure was steady under a certain numbers of fatigue loadings (figure 7). When the pressure reached 15 N, CPE_1-T rose sharply once after 8000 times' fatigue loading. With the increase of pressure, the micro damage on the MRE-electrode interface layer happened earlier.

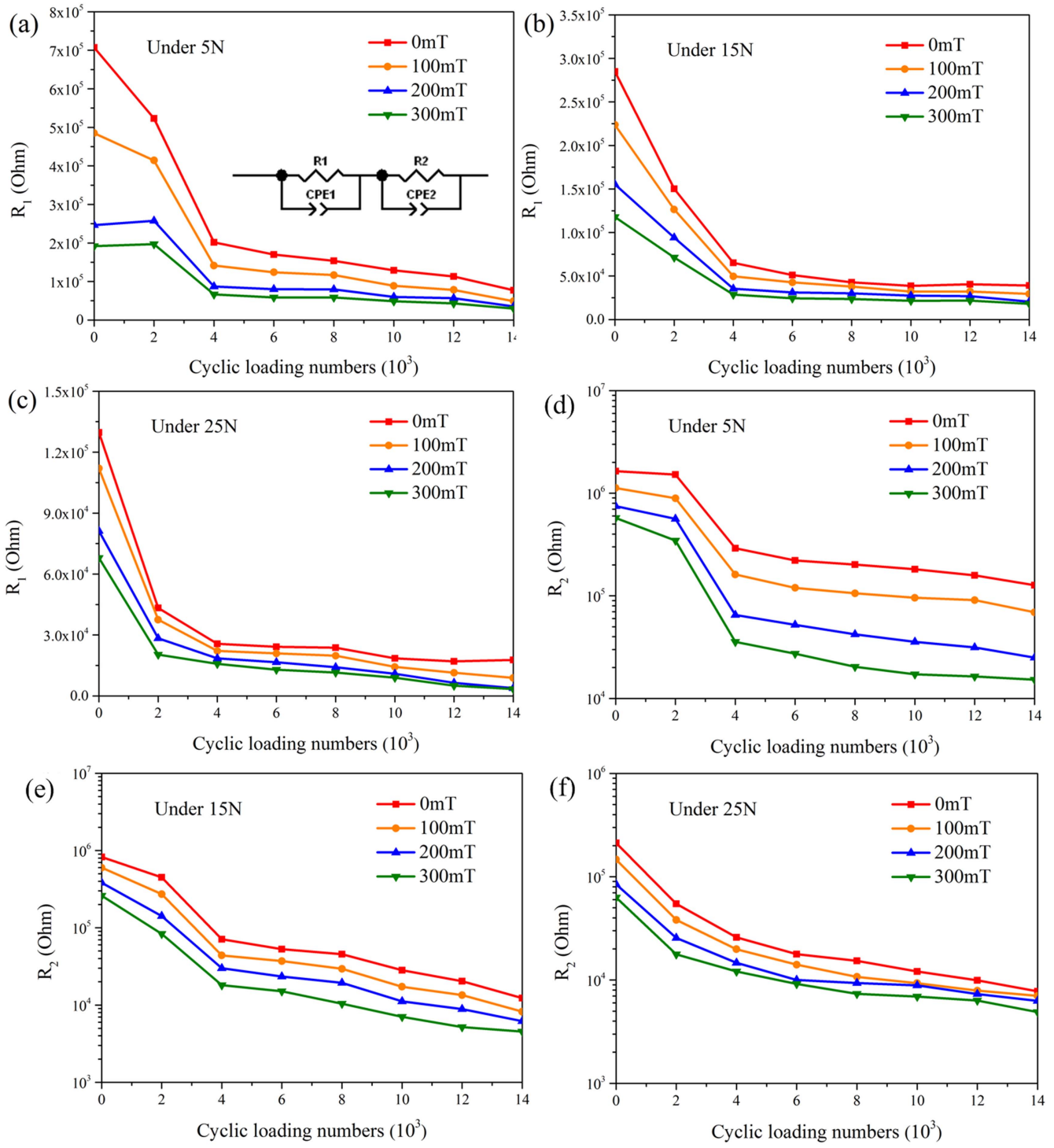

Figure 8. The relationship between the resistance elements and cyclic loading numbers under different testing conditions: (a) R_1-5 N; (b) R_1-15 N; (c) R_1-25 N; (d) R_2-5 N; (e) R_2-15 N; (f) R_2-25 N.

When the pressure reached 25 N, it could be seen that without fatigue loading, there was a certain degree of damage happened, thus CPE_1-T increased at the beginning of the test.

CPE_2-T represented the capacitance of the main specimen. Because the particles content reached as high as 85 wt%, the microstructure of MRE became to change once after 2000 times fatigue loading (figures 9(d)–(f)). When the MRE was under 5 N, after a stable stage between 4000 times and 10 000 times' loading, the CPE_2-T rose greatly. This was similar to the figure 5. In practice, we can detect the change even damage of MREs real-time and nondestructive through this method, predict the operation life, and judge the type and degree of fatigue or damage.

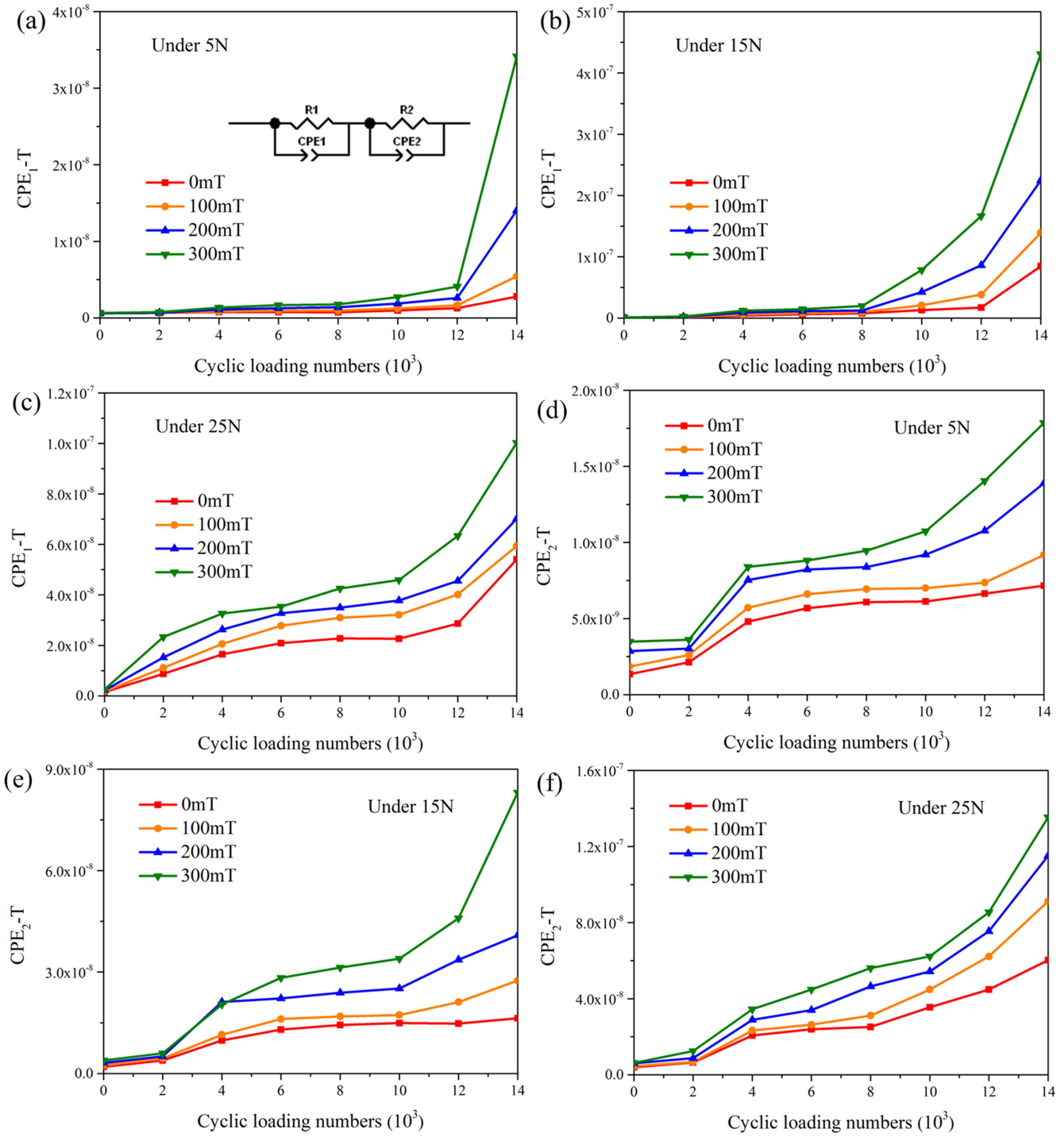

Figure 9. The relationship between the constant phase angle elements and cyclic loading numbers under different testing conditions: (a) CPE_1-T-5 N; (b) CPE_1-T-1 5 N; (c) CPE_1-T-25 N; (d) CPE_2-T-5 N; (e) CPE_2-T-15 N; (f) CPE_2-T-25 N.

4. Conclusion

In this work, natural rubber based MREs with 85 wt% of iron particles were prepared, and then endured 0–14 000 times' fatigue loading. With increasing of the cyclic loading numbers, the sweeping frequencies have a greater impact on the shear storage modulus. The modulus had a slow rise process after 1×10^4 times cyclic loading. There were two reasons: firstly, the destruction of the microstructure and the slippage happened; Secondly, with the degree of the fatigue increased, the plastic deformation was more and more obvious.

When pressure was less than 10 N, the curves of capacitance could be divided into four sections with the cyclic loading numbers. The greater the magnetic field strength, the more obvious these performance. A coupling effect was found between the electrical performance and mechanical performance. The platform segments of curves corresponding to the yield stage of MRE. The distortion of structure caused

by internal stress got released and recovered after a certain degree of fatigue loading. The MRE without the fatigue load was less affected by the external magnetic field. Due to the Magnetic contraction, particles gradually move towards the sample center area. It could be regarded that the specimen consisted of two different components: the MRE center area and the MRE-electrode interface layer. An equivalent circuit model was established to fit and analyze the electric response of MRE samples under different external stimuli. Thus, the MRE properties and the change of the microstructure could be obtained and analyzed. The place where fully compression happened first when loading force was the MRE-electrode interface layer. It could be considered that the interface had been damaged after 12 000 times loading when pressure was 5 N. With the increase of pressure, the micro damage on the MRE-electrode interface layer happened earlier. Pressure loading and magnetic contraction had different influence on the MRE and MRE-electrode interface layer. On account of the application in vibration, this method can be used to detect the MRE's micro damage, and predict the service life.

Acknowledgments

Financial support from the National Natural Science Foundation of China (Grant Nos. 11572309, 11572310) and the Fundamental Research Funds for the Central Universities (WK2480000002) are gratefully acknowledged. This work was also supported by Collaborative Innovation Center of Suzhou Nano Science and Technology.

References

[1] Jung H S, Kwon S H, Choi H J, Jung J H and Kim Y G 2016 Magnetic carbonyl iron/natural rubber composite elastomer and its magnetorheology *Compos. Struct.* **136** 106–12
[2] Yu M, Ju B X, Fu J, Liu X Q and Yang Q 2012 Influence of composition of carbonyl iron particles on dynamic mechanical properties of magnetorheological elastomers *J. Magn. Magn. Mater.* **324** 2147–52
[3] Sun S S, Deng H X, Yang J, Li W H, Du H P, Alici G and Nakano M 2015 An adaptive tuned vibration absorber based on multilayered MR elastomers *Smart Mater. Struct.* **24** 045045
[4] Choi S B, Li W H, Yu M, Du H P, Fu J and Do P X 2016 State of the art of control schemes for smart systems featuring magneto-rheological materials *Smart Mater. Struct.* **25** 043001
[5] Nayak B, Dwivedy S K and Murthy K S R K 2014 Dynamic stability of a rotating sandwich beam with magnetorheological elastomer core *Eur. J. Mech.* A **47** 143–55
[6] Nayak B, Dwivedy S K and Murthy K S R K 2011 Dynamic analysis of magnetorheological elastomer-based sandwich beam with conductive skins under various boundary conditions *J. Sound Vib.* **330** 1837–59
[7] Li Y C, Li J C, Li W H and Samali B 2013 Development and characterization of a magnetorheological elastomer based adaptive seismic isolator *Smart Mater. Struct.* **22** 035005
[8] Li Y C, Li J C, Li W H and Du H P 2014 A state-of-the-art review on magnetorheological elastomer devices *Smart Mater. Struct.* **23** 123001
[9] Brosseau C, Mdarhri A and Vidal A 2008 Mechanical fatigue and dielectric relaxation of carbon black/polymer composites *J. Appl. Phys.* **104** 074105
[10] Le Cam J B, Huneau B, Verron E and Gornet L 2004 Mechanism of fatigue crack growth in carbon black filled natural rubber *Macromolecules* **37** 5011–7
[11] Kim J H and Jeong H Y 2005 A study on the material properties and fatigue life of natural rubber with different carbon blacks *Int. J. Fatigue* **27** 263–72
[12] Abraham F, Alshuth T and Jerrams S 2005 The effect of minimum stress and stress amplitude on the fatigue life of non strain crystallising elastomers *Mater. Des.* **26** 239–45
[13] Zhang W, Gong X L, Jiang W Q and Fan Y C 2010 Investigation of the durability of anisotropic magnetorheological elastomers based on mixed rubber *Smart Mater. Struct.* **19** 085008
[14] Zhang W, Gong X L, Sun T L, Fan Y C and Jiang W Q 2010 Effect of cyclic deformation on magnetorheological elastomers *Chin. J. Chem. Phys.* **23** 226–30
[15] Zhou Y F, Jerrams S and Chen L 2013 Multi-axial fatigue in magnetorheological elastomers using bubble inflation *Mater. Des.* **50** 68–71
[16] Zhou Y F, Jerrams S, Betts A and Chen L 2014 Fatigue life prediction of magnetorheological elastomers subjected to dynamic equi-biaxial cyclic loading *Mater. Chem. Phys.* **146** 487–92
[17] Bica I 2010 Magnetorheological elastomer-based quadrupolar element of electric circuits *Mater. Sci. Eng.* B **166** 94–8
[18] Bica I 2012 The influence of hydrostatic pressure and transverse magnetic field on the electric conductivity of the magnetorheological elastomers *J. Ind. Eng. Chem.* **18** 483–6
[19] Bica I, Liu Y D and Choi H J 2012 Magnetic field intensity effect on plane electric capacitor characteristics and viscoelasticity of magnetorheological elastomer *Colloid Polym. Sci.* **290** 1115–22
[20] Bica I 2009 Influence of magnetic field upon the electric capacity of a flat capacitor having magnetorheological elastomer as a dielectric *J. Ind. Eng. Chem.* **15** 605–9
[21] Ghafoorianfar N, Wang X J and Gordaninejad F 2014 Combined magnetic and mechanical sensing of magnetorheological elastomers *Smart Mater. Struct.* **23** 055010
[22] Bunoiu M and Bica J 2016 Magnetorheological elastomer based on silicone rubber, carbonyl iron and Rochelle salt: effects of alternating electric and static magnetic fields intensities *J. Ind. Eng. Chem.* **37** 312–8
[23] Ausanio G, Iannotti V, Ricciardi E, Lanotte L and Lanotte L 2014 Magneto-piezoresistance in magnetorheological elastomers for magnetic induction gradient or position sensors *Sensors Actuators* A **205** 235–9
[24] Borin D Y and Stepanov G V 2015 Elastomer with magneto- and electrorheological properties *J. Intell. Mater. Syst. Struct.* **26** 1893–8
[25] Yu M, Yang P A, Fu J, Liu S Z and Choi S B 2016 A theoretical model for the field-dependent conductivity of magneto-rheological gels and experimental verification *Sensors Actuators* A **245** 127–34
[26] Tian T F, Li W H and Alici G 2013 Study of magnetorheology and sensing capabilities of MR elastomers *J. Phys.: Conf. Ser.* **412** 025022
[27] Ausanio G, Barone A C, Campana C, Iannotti V, Luponio C, Pepe G P and Lanotte L 2006 Giant resistivity change induced by strain in a composite of conducting particles in an elastomer matrix *Sensors Actuators* A **127** 56–62
[28] Kchit N, Lancon P and Bossis G 2009 Thermoresistance and giant magnetoresistance of magnetorheological elastomers *J. Phys. D: Appl. Phys.* **42** 105506

[29] Ausanio G, Hison C L, Iannotti V, Lanotte L and Lanotte L 2011 Magneto-piezoresistance in elastomagnetic composites *J. Appl. Phys.* **110** 063903
[30] Ju B X, Tang R, Zhang D Y, Yang B L, Yu M, Liao C R, Yuan X L, Zhang L W and Liu J H 2016 Dynamic mechanical properties of magnetorheological elastomers based on polyurethane matrix *Polym. Compos.* **37** 1587–95
[31] Yu M, Qi S, Fu J and Zhu M 2015 A high-damping magnetorheological elastomer with bi-directional magnetic-control modulus for potential application in seismology *Appl. Phys. Lett.* **107** 035005
[32] Yu M, Fu J, Ju B X, Zheng X and Choi S B 2013 Influence of x-ray radiation on the properties of magnetorheological elastomers *Smart Mater. Struct.* **22** 125010
[33] Qiao X Y, Lu X S, Gong X L, Yang T, Sun K and Chen X D 2015 Effect of carbonyl iron concentration and processing conditions on the structure and properties of the thermoplastic magnetorheological elastomer composites based on poly(styrene-b-ethylene-co-butylene-b-styrene) (SEBS) *Polym. Test.* **47** 51–8
[34] Gunther D, Borin D Y, Gunther S and Odenbach S 2012 X-ray micro-tomographic characterization of field-structured magnetorheological elastomers *Smart Mater. Struct.* **21** 015005
[35] Borbath T, Gunther S, Borin D Y, Gundermann T and Odenbach S 2012 XμCT analysis of magnetic field-induced phase transitions in magnetorheological elastomers *Smart Mater. Struct.* **21** 105018
[36] Gundermann T and Odenbach S 2014 Investigation of the motion of particles in magnetorheological elastomers by X-μCT *Smart Mater. Struct.* **23** 105013
[37] Wang Y, Xuan S H, Dong B, Xu F and Gong X L 2016 Stimuli dependent impedance of conductive magnetorheological elastomers *Smart Mater. Struct.* **25** 025003
[38] Xu Y G, Gong X L, Liu T X and Xuan S H 2013 Magneto-induced microstructure characterization of magnetorheological plastomers using impedance spectroscopy *Soft Matter* **9** 7701–9
[39] Wang X J, Gordaninejad F, Calgar M, Liu Y M, Sutrisno J and Fuchs A 2009 Sensing behavior of magnetorheological elastomers *J. Mech. Des.* **131** 091004
[40] Ge L, Gong X L, Fan Y C and Xuan S H 2013 Preparation and mechanical properties of the magnetorheological elastomer based on natural rubber/rosin glycerin hybrid matrix *Smart Mater. Struct.* **22** 115029
[41] Saji J, Khare A and Mahapatra S P 2015 Impedance and dielectric spectroscopy of nano-graphite reinforced silicon elastomer nanocomposites *Fibers Polym.* **16** 883–93
[42] Kchit N and Bossis G 2009 Electrical resistivity mechanism in magnetorheological elastomer *J. Phys. D: Appl. Phys.* **42** 105505